Supplemental information

Section 1: Spectral fitting[1]

The spectral fitting protocol is described in ref 1. The data (appearing, in part, in ref 1) are summarized in the following tables:

Table S1. Spectral fitting parameters for $L_M Zn$ MOF.

sample	E_0 / cm^{-1}	$\nu_{1/2}$ / cm^{-1}	$\hbar\omega_M$ / cm^{-1}	S_M	r	λ / cm^{-1}
$L_{Ru}Zn$ MOF	15598	1693	1317	0.77	0.99967	2263
$L_M Zn$ *2.6 % Os* MOF	13819	1048	1093	0.72	0.99553	1262

Table S2. Spectral fitting parameters for $L_M Zn$-*Ox* MOF.

sample	E_0 / cm^{-1}	$\nu_{1/2}$ / cm^{-1}	$\hbar\nu_M$ / cm^{-1}	S_M
$L_{Ru}Zn$-*Ox* MOF	17781	717	1283	0.97
$L_{Os}Zn$-*Ox* MOF	14137	899	998	0.98

Section 2: Os excited state lifetime

The experimentally measured 259 ns Os excited state lifetime in $L_M Zn$-*Ox* MOF [1] rests on the assumption that the Ru-to-Os energy transfer can be neglected at long times when the Ru emission is very weak. This can be interpreted as an excited state population $P_{Os^{II*}}(t)$ on Os at time *t*:

$$P_{Os^{II*}}(t) = \int_0^t p_{Ru\to Os}(\tau)\exp\left(-(t-\tau)/\tau_{Os^{II*}}\right)d\tau \qquad (1)$$

where $p_{Ru\to Os}(\tau)$ is the exciton population transfer rate to Os at time τ. When $p_{Ru\to Os}(\tau) = 0$, the exciton population on Os reflects its lifetime. Simulations were carried out to validate this assumption by computing the ratio $\gamma(t)$ of the total excition transfer rate from Ru to Os to the rate of Os decay as a function of time:

$$\gamma(t) = \frac{k_{Ru\to Os}P_{Ru^*}(t)}{k_{Os}^{dec}P_{Os^*}(t)} \qquad (2)$$

Here, $P_{Ru^*}(t)$ and $P_{Os^*}(t)$ are excition populations on Ru and Os at time t, $k_{Ru\to Os}$ is the energy transfer rate from Ru to a neighboring Os, and k_{Os}^{dec} is the Os exciton decay rate. $\gamma(t)$ is shown in Fig. S1. These results indicate that the assumption for obtaining

the lifetime of the Os excited state is not validated. Thus, 259 ns for Os excited state lifetime is an over estimate.

Table S1: Single site energy transfer rates, Ru and Os excited states lifetimes for 1.16% Os doping, and Os excited state lifetimes in the L_M*Zn-Ox* MOF that reproduce experimentally measured Ru and Os measured emission.

τ_{Os^*}	Os%	τ_{Ru^*}	$k_{Ru\rightarrow Ru}$	$k_{Ru\rightarrow Os}$	$k_{Os\rightarrow Os}$	$P_{i=Ru}(0)/P_{i=Os}(0)$
259ns	1.16	73ns	$(50ns)^{-1}$	$(106ns)^{-1}$	$(50ns)^{-1}$	0.5

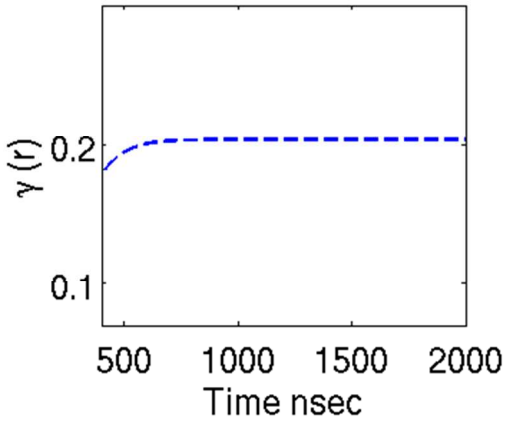

Figure S1: Ratio of the rate of exciton flowing into all Os sites to the rate of excitation that decay on all Os sites as a function of time in the L_M*Zn-Ox* MOF. Data are computed with energy transfer rates and Ru and Os excited state lifetime listed in Table S1.

Section 3: Possible origins of the Ru excited-state lifetime change in the low Os doping regime.

The significant change of the Ru lifetime from the pure Ru MOF to the lightly Os doped Ru MOF for both MOF structures suggests an additional excited state quenching mechanism. We explore the possibility of: a) Os clustering, b) long range Förster energy transfer.

(a) Os Clustering

Simulations of Ru and Os transient emission in the two MOF structures described above are based on homogenous Os distributions. One would expect that clustered Os

distribution would reduced the Ru lifetime in Os doped MOFs in the vicinity of higher Os levels. A simulation is carried out to test this hypothesis. The protocol for this simulation is: 1) energy transfer rates (see Table S3) for Ru-to-Ru and Ru-to-Os are determined by fitting both Ru and Os time-dependent emission for 1.4% Os doped L_MZn MOFs (see Fig. S4) and the rates are then used for the 2.6% Os doping case with Os clustering (see Fig. S5).

Table S2: Nearest-neighbor energy transfer rates and Ru and Os excitation lifetimes for different Os doping levels in the L_MZn based MOF.

Os%	τ_{Ru^*}	τ_{Os^*}	$k_{Ru\to Ru}$	$k_{Ru\to Os}$	$k_{Os\to Os}$	$P_{i=Os}(0)/P_{i=Ru}(0)$
1.4	26 ns	8 ns	$(0.3\ \text{ns})^{-1}$	$(15.6\ \text{ns})^{-1}$	$(0.3\ \text{ns})^{-1}$	0.10
2.6	26 ns	8 ns	$(0.3\ \text{ns})^{-1}$	$(15.6\ \text{ns})^{-1}$	$(0.3\ \text{ns})^{-1}$	0.10

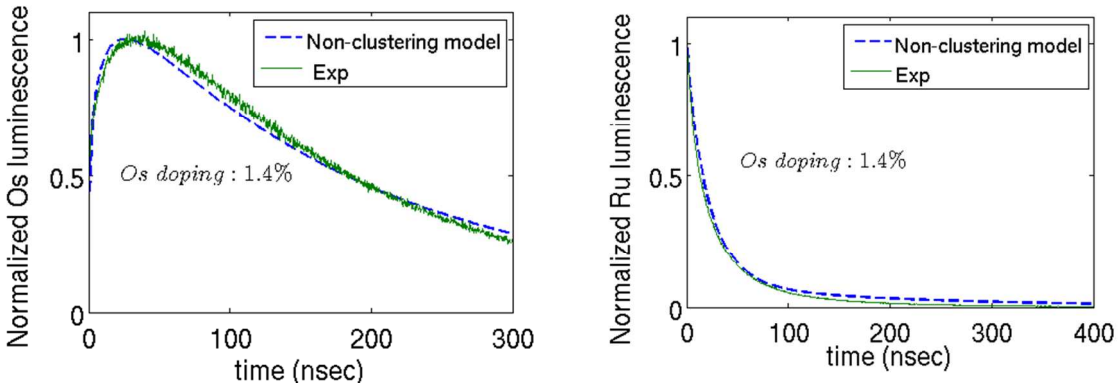

Figure S4: Comparison of experimental and simulated Ru and Os emission with 1.4% Os doped L_MZn MOFs with energy transfer rates and Ru/Os lifetimes in Table S2. The Os distribution is assumed homogenous. The experimentally observed zero time emission was corrected by setting the initial excitation population on Ru and Os to be 0.1. Each ensemble member contains 6,000 Ru/Os sites in one dimension. The ensemble averaged time-resolved emission was obtained with a numerical convergence of 0.01%

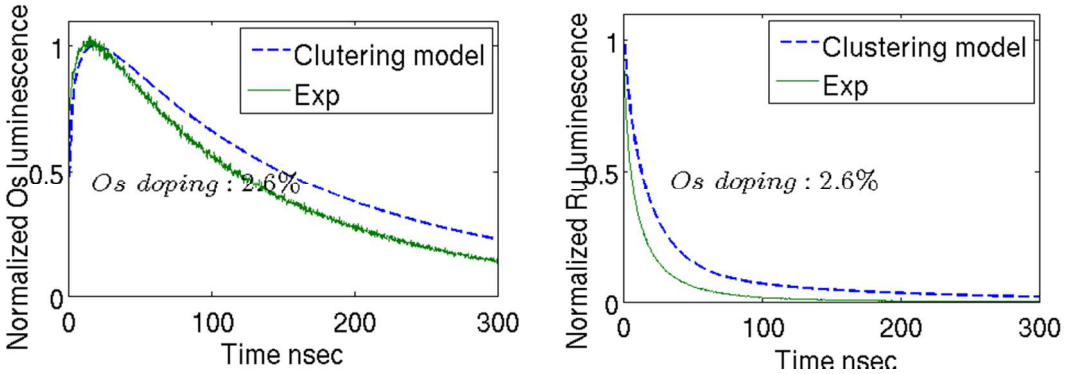

Figure S5: Comparison of experimental and simulated Ru and Os emission with 1.4% Os doped L_MZn MOF with energy transfer rates and Ru/Os lifetime list in Table S2. The Os sites are clustered. Os sites were placed in pairs. The experimentally observed zero time emission was corrected by setting the initial excitation population on Ru and Os to be 0.1. The computed time-resolved emission was the average of ensemble members with the noted Os doping level. Each ensemble member contains 6000 Ru/Os complexes. The converged averaged time-resolved emission was obtained with numerical converge tolerance 0.01%.

To consider "strong" Os sites clustering effect, Os sites were constructed in pairs with one Ru site between Os sites, the Ru lifetime in the 2.6% Os doped L_MZn MOF does not shorten in to the extend observed experimentally. Thus, Os clustering cannot explain the significant Ru lifetime shortening. In fact, clustering of Os would give each Os a diminished quenching yield, due to fewer accessible Ru excited states (see discussion below). Therefore, Ru-to-Os energy transfer with Os clustering produces longer Ru excited-state lifetimes. However, clustering of Os will shorten the Os emission peak time, i.e in the simulated time-resolved emission plot of Figs. S4 and S5, the Os emission peak time is shorter in the 2.6% doping case.

(b) Os time-resolved emission peak time shortening and Os clustering

Energy transfer in the 1D MOF with homogenously distributed Os sites is described schematically in Fig. S6,

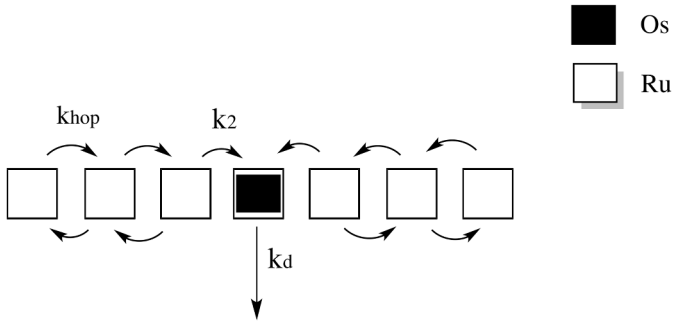

Figure S6

A short chain model of the energy transfer is adapted to simplify the analysis. Here, k_{hop} is the energy transfer rate between nearest-neighbor Ru sites**,** k_2 is the energy trapping rate from Ru to Os sites, and k_d is the Os excited state decay rate. There are six Ru sites and one Os site in total. We assume all Ru sites are excited and there are six excitons created. Our aim is to obtain the exciton population on the Os site as a function of time and to compute the corresponding peak position in the Os emission spectrum with and without Os clustering. Without clustering, we can further reduce the Ru chain to an effective model as shown in Fig. S7

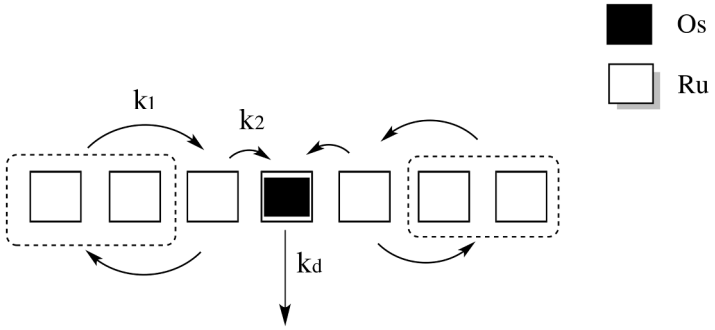

Figure S7

Since only Ru next to Os deliver excitons to the Os site, we explicitly focus on this type of Ru site ("nearest-neighbor Ru"). The other Ru sites only deliver excitons to the "nearest-neighbor Ru". Therefore, non-nearest-neighbor Ru can be treated as an effective exciton reservoir. In this model, k_1 is the effective energy transfer rate between nearest-neighbor Ru and non-nearest-neighbor Ru, k_2 is the energy trapping rate from nearest-neighbor Ru to Os site, and k_d is the Os excited state decay rate. Here, the left and right side exciton transfer processes are equivalent and act independently. Thus, this energy transfer chain can be further simplified as a three sites model shown in the Fig. S8 with

doubled exciton populations on the nearest-neighbor Ru and non-nearest-neighbor Ru compared to the full picture in Fig. S7.

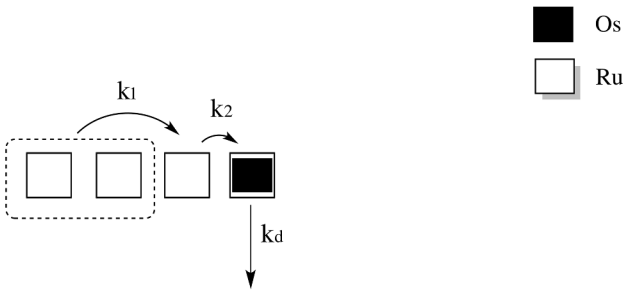

Figure S8

The time-dependent Os* population can be calculated by solving the energy transfer kinetic equation

$$d\begin{pmatrix} P_1(t) \\ P_2(t) \\ P_3(t) \end{pmatrix} / dt = \begin{bmatrix} -k_1 & k_1 & 0 \\ k_1 & -k_1 - k_2 & 0 \\ 0 & k_2 & -k_3 \end{bmatrix} \cdot \begin{pmatrix} P_1(t) \\ P_2(t) \\ P_3(t) \end{pmatrix} \quad (3)$$

where $P_1(t)$, $P_2(t)$ and $P_3(t)$ are the time-dependent exciton populations on non-nearest-neighbor Ru, nearest-neighbor Ru, and Os. The initial excitation population is $\{P_1(0)=4, P_2(0)=2, P_3(0)=0\}$. The peak time in the time-resolved emission is obtained by solving $dP_3(t)/dt = 0$.

The clustering model we employed is shown schematically in Fig. S9.

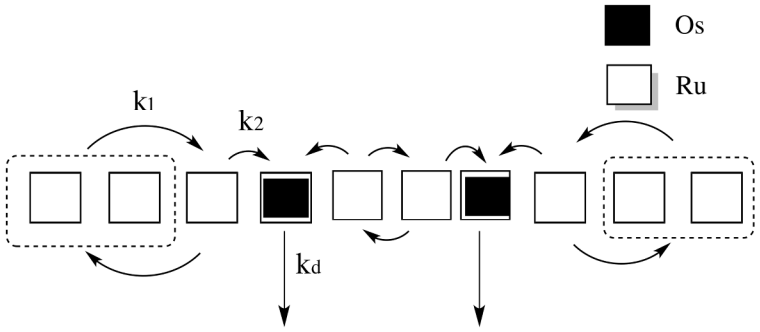

Figure S9

To simplify the analysis, we introduce the clustering of Os with two Ru sites in between. For each Os, the energy transfer on the left and right sides is no longer equivalent because of the Os clustering and the irreversible Os trapping. There is no net energy flow

between two Os sites. Therefore, the model can be reduced to an effective one as shown in Fig. S10:

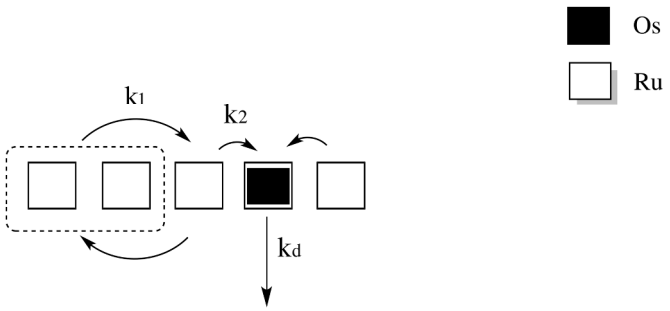

Figure S10

Comparing this energy transfer diagram with the homogenous one, the only difference is that the initial exciton population on the non-nearest-neighbor Ru. That is, the initial excitation population changes to $\{P_1(0)=2, P_2(0)=2, P_3(0)=0\}$. With this kinetic model, the peak time may be computed. With k_1= (50 ns)$^{-1}$, k_2=(106 ns)$^{-1}$ and k_3=(150 ns)$^{-1}$, the typical values we used in our MOF simulations, the peak time for the homogenously distributed Os model is 194 ns, and is 184 ns for the clustering model. The shifting of the Os emission peak to earlier time arises because the exciton population for each Os is effectively reduced by Os clustering.

(c) Long-range Förster energy transfer

Long-range energy transfer could enhance the flow of excitons to Os traps. This idea was tested by simulating Ru and Os transient emission in Os doped L_MZn MOFs. The simulation procedure was: 1) we add to the nearest neighbor hopping model an additional Förster type distance dependent energy transfer rate with $k(r) = k(R_0)(R/R_0)^{-6}$, where $k(R_0)$ is the nearest-neighbor energy transfer rate, and R_0 is the distance between nearest-neighbor sites (see Table S4). We considered an extreme case of all Ru excited states singlet multiplicity and a very strong Förster coupling strength comparable with the computed Dexter coupling; 2) we determined the site-to-site energy transfer rates by fitting both Ru and Os time-resolved transient emission from 1.4% Os doping case (see Fig. S11); 3) we used the fitted site-to-site energy transfer rate to simulate the Ru and Os time-resolved transient emissions for 2.6% Os doped MOF (see Fig. S12). Fig. S12 shows that Förster energy transfer cannot account for the change in the Ru lifetime as the

Os doping level increases. The simulations indicated that Förster energy transfer does not enhance the accumulation of excitions on Os, in contrast to the experiments. In other words, the small long-range energy transfer contribution arises from the $(R/R_0)^{-6}$ factor that scales the energy transfer rate. Therefore, the long-range energy transfer mechanism causes little change in the kinetics from the single site hopping model when describing the Ru excited-state lifetime.

Table S3: Single site energy transfer rates and Ru and Os excitation lifetimes for different Os doping levels for L_MZn MOF.

Os%	τ_{Ru^*}	τ_{Os^*}	$k_{Ru\rightarrow Ru}$	$k_{Ru\rightarrow Os}$	$k_{Os\rightarrow Os}$	$P_{i=Os}(0)/P_{i=Ru}(0)$
1.4	26 ns	8 ns	$(0.33\ \text{ns})^{-1}$	$(15.5\ \text{ns})^{-1}$	$(0.33\ \text{ns})^{-1}$	0.10
2.6	26 ns	8 ns	$(0.33\ \text{ns})^{-1}$	$(15.5\ \text{ns})^{-1}$	$(0.33\ \text{ns})^{-1}$	0.10

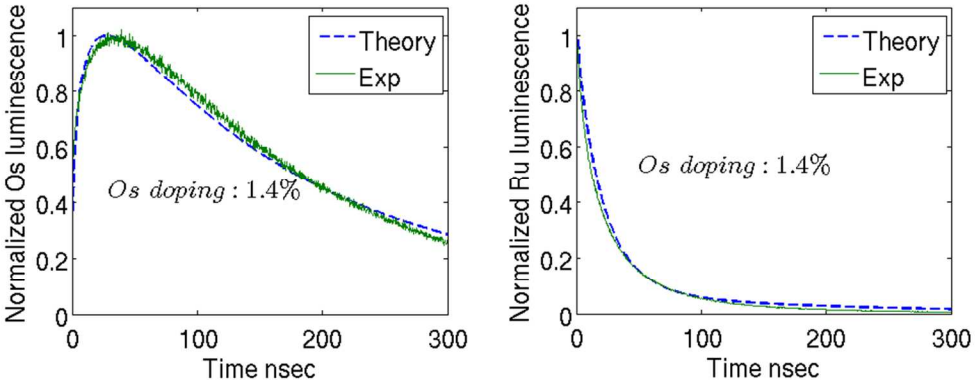

Figure S11: Comparison of experimental and simulated Ru and Os emission with 1.4% Os doped L_MZn MOFs based upon energy transfer rates and Ru/Os lifetimes in Table S3, assuming a Förster energy transfer mechanism. The Os distribution was assumed homogenous. The experimentally observed zero time emission was corrected by setting the initial excitation population on Ru and Os to 0.1. Each ensemble member contains 6,000 Ru/Os complexes aligned in one dimension. The converged ensemble averaged time-resolved emission was obtained with a tolerance of 0.01%.

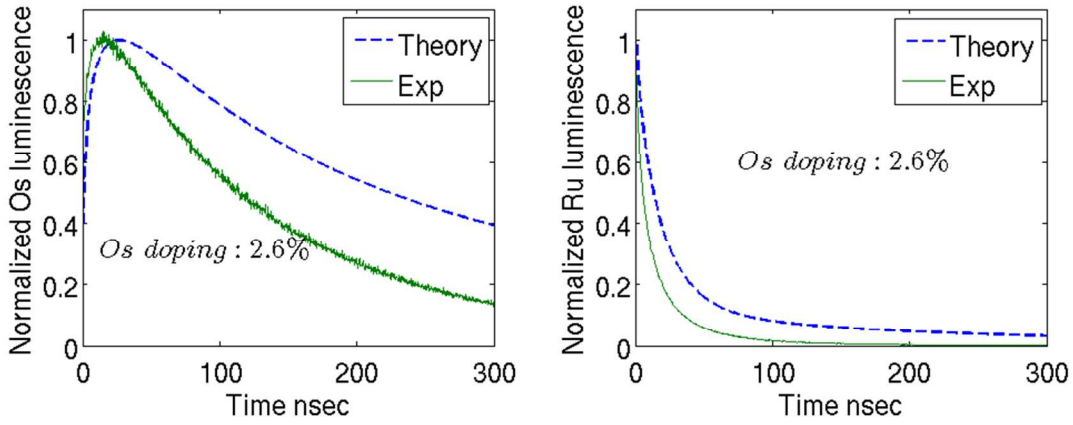

Figure S12: Comparison of experimental and simulated Ru and Os emission including long range energy transfer with 2.6% Os doped L_MZn MOFs and energy transfer rates and lifetimes in Table S3. The Os distribution is assumed homogenous. Each ensemble member contains 6,000 Ru/Os complexes aligned in one dimension. The converged ensemble averaged time-resolved emission was obtained with a tolerance of 0.01%.

The two postulated explanations proved unable to explain the change of Ru lifetime with Os doping level. Clustering of Os shortens the Os peak emission time by reducing the number of accessible Ru excitations surrounding each Os. Simulations of long-range Förster energy transfer is not able to accelerate Ru exciton arrivas at Os sites to account for the change of the Ru lifetime with increased Os doping.

Section 4: Energy transfer efficiency normalized by exciton diffusion length

(a) Diffusion length of an exciton in 1D energy transfer network

In MOF with 1D and 3D energy transfer networks, energy trapping at Os is a proxy for energy harvesting efficiency. We define γ as the ratio of exciton transported to Os sites to the total number of excitons created on Ru sites within the exciton diffusion length l. In both MOFs, energy transfer is defined by the exciton diffusion length. The exciton diffusion length is the root mean square distance that an exciton can hop during its lifetime. Unbiased exciton diffusion can be considered as a random walk. The mean number of walk steps N that an exciton can make during its lifetime τ with a nearest-neighbor energy transfer rate k is:

$$N = k\,\tau \qquad (4)$$

Therefore, for the 1D energy transfer network, the diffusion length is calculated [1, 2] as:

$$L_1 = \sqrt{Na^2} \qquad (5)$$

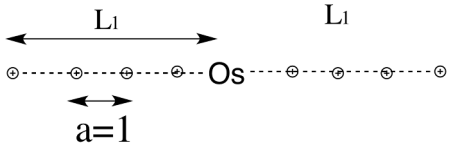

Figure S13

where *a = 1* is the distance between two nearest-neighbor Ru/Os sites. For a given Os in a MOF with a 1D energy transfer network, the number of sites within the range of a diffusion length for this Os is $\boldsymbol{2L_1}$ (here we assume no overlap of diffusion length range between different Os sites.). Between $-L_1$ and L_1, only $\boldsymbol{L_1}$ excitons can finally be trapped at the Os site (Fig. S13).

Therefore, in the low Os doping regime, where the distance between two Os sites is much larger than the diffusion length, each Os can trap $\boldsymbol{L_1}$ excitons if all of the Ru sites were excited. Thus, within the range of diffusion length L_1:

$$\gamma_{1D} = \frac{L_1}{2L_1} = \frac{1}{2} \qquad (6)$$

(b) Diffusion length of an exciton in a 3D energy transfer network

The average number of random walk steps that an exciton can make during its lifetime is:

$$N = k\,\tau \qquad (7)$$

During the lifetime of an exciton, *N/3* steps of the random walk will occur along each axis. Therefore, the root mean square distance along each axis from the origin of the exciton is

$$L_{3(x)} = L_{3(y)} = L_{3(z)} = \sqrt{Na^2/3}\,\tau \qquad (8)$$

where *a=1* is the distance between two nearest-neighbor Ru/Os sites. Therefore, the diffusion length is:

$$L_3 = \sqrt{(L_{3(x)}^2 + L_{3(y)}^2 + L_{3(z)}^2)} = \sqrt{N}\,\tau \qquad (9)$$

In the low Os doping regime, the excitons that will arrive at an Os are within a sphere range around Os with radius L_3. How many excitons in this sphere will reach the centeral Os?

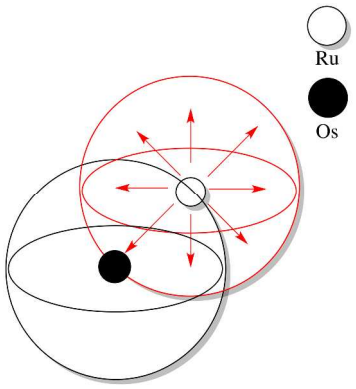

Figure S14

Assuming that an excition within this sphere is located at radius R. After N hopping steps, this exciton would be distributed evenly on a sphere centered at the source of this exciton with radius $r = \sqrt{N}$ (the sphere with red arrows in Fig. S14). The possibility of this exciton being trapped at the centeral Os (as shown in the Fig. S14) is given by the ratio of the total number of sites on this spherical surface to the Os shown in Fig. S14:

$$P(R) = \frac{1}{Total\ sites\ on\ the\ red\ sphere\ surface} = \frac{1}{F(R)} \qquad (10)$$

There total number of Ru sites that are R from the Os is $F(R)$. Therefore, the number of excitons that arrive at the Os site from the spherical surface with radius R is:

$$n(R) = P(R)F(R) = 1 \qquad (11)$$

Therefore, in the sphere with radius equal to the diffusion length with Os as its origin, if all Ru sites are excited, the number of excitons to reach Os is:

$$P_{\square otal} = \int_0^{L_3} n(R)dR = L_3 \qquad (12)$$

Therefore, only L_3 excitons within this sphere are trapped by the Os. Therefore,

$$\gamma_{3D} = \frac{L_3}{(4/3)\pi L_3^3} \qquad (13)$$

$\gamma_{1D}$is much less than γ_{3D}. Moreover, in a 1D energy transfer network, one would expect to capture all the excitons on the Ru by creating a MOF with a distance $\boldsymbol{L_1}$ between all nearest-neighbor Os sites in the network.

References:

1. Spectral fitting was kindly provided by Dr. Akitaka Ito. See also: Kent, C.A.; Liu, D.; Ito, A.; Zhang, T.; Brennaman, M.K.; Meyer, T.J.; and Lin, W. J. Mater. Chem. A., submitted 2013.

2. Kent, C.A. Photo-active and redox-active metal-organic frameworks for solar energy utilization. Ph.D., The University of North Carolina at Chapel Hill at Chapel Hill, 2012.

3. Pope, M.; Swenberg, C.E. Electronic processes in organic crystals and polymers, Oxford University Press: New York; 1999, Ch. I.F, G.□

4. Agranovich, V. M. Excitations in organic solids, Oxford University Press: New York, 2008; Ch. 2,14.